Plasmonics (2013) 8:1627–1631
DOI 10.1007/s11468-013-9580-4

Coupled-Resonator-Induced Fano Resonances for Plasmonic Sensing with Ultra-High Figure of Merits

Jianjun Chen · Zhi Li · Yujiao Zou · Zhongliang Deng · Jinghua Xiao · Qihuang Gong

Received: 28 February 2013 / Accepted: 14 May 2013 / Published online: 24 May 2013

Abstract Fano resonances are numerically predicted in an ultracompact plasmonic structure, comprising a metal-isolator-metal (MIM) waveguide side-coupled with two identical stub resonators. This phenomenon can be well explained by the analytic model and the relative phase analysis based on the scattering matrix theory. In sensing applications, the sensitivity of the proposed structure is about 1.1×10^3 nm/RIU and its figure of merit is as high as 2×10^5 at $\lambda=980$ nm, which is due to the sharp asymmetric Fano line-shape with an ultra-low transmittance at this wavelength. This plasmonic structure with such high figure of merits and footprints of only about 0.2 μm^2 may find important applications in the on-chip nano-sensors.

Keywords Surface plasmon polaritons · Coupled resonators · Fano resonances · Sensor · Phase analysis

Introduction

Fano resonances in metallic nanostructures are a coupling effect which results from the interaction of narrow dark modes with broad bright modes [1–3]. Different from the Lorentzian resonances emerging in universal resonators, the Fano resonances exhibit sharp and asymmetric spectral line-shapes together with strong field enhancements, which have potential applications in the areas of nonlinearities, lasing, modulators, and biosensors [1–4]. In the past decade, tremendous attentions were attracted to design various metallic structures to generate the Fano resonances. For example, the plasmonic array structures ranging from particle lattices and oligomers to nano-wire lattices and split-ring type structures [5–17] were proposed to realize Fano resonances. For highly integrated photonic circuits, these array structures are a little bulky and complicated, making them hard to be integrated into chips. Recently, using a unit-cell structure side-coupled with detuned resonators, the Fano resonances were also theoretically predicted [18–27] and even experimentally demonstrated [4, 28]. Compared with the array structures, the unit-cell plasmonic structures are much compact and easy to be integrated into chips. In any event, because of the sharp asymmetric response line-shapes together with the strong field enhancements in the Fano resonances, all of these metallic structures exhibit high sensitivity to the index variations of nearby or surrounding medium, showing great prospect in the applications of nano-plasmonic sensors [1, 2, 12, 28, 29].

In the paper, Fano resonances are obtained in an ultracompact plasmonic structure, comprising a metal-isolator-metal (MIM) waveguide [21–23, 26] side-coupled with two identical stub resonators. Near the resonant wavelength of the stub resonator, the surface plasmon polaritons (SPPs) [21–23, 26] guided by the MIM waveguide can be highly reflected. Consequently, the SPPs at these wavelengths can be highly reflected back and forth off the two identical stub resonators, constructing a Fabry–Perot (FP) resonator [18, 26] in the plasmonic system. Because of the high reflectivity, a strong trapped resonance with a narrow bandwidth is excited in the FP resonator. Herein, the

J. Chen · Z. Deng · J. Xiao
State Key Laboratory of Information Photonics and Optical Communications, Beijing University of Posts and Telecommunications, Beijing 100876, China

J. Chen (✉) · J. Xiao
School of Science, Beijing University of Posts and Telecommunications, Beijing 100876, China
e-mail: chernmore@pku.edu.cn

Z. Li · Q. Gong
State Key Laboratory for Mesoscopic Physics and Department of Physics, Peking University, Beijing 100871, China

Y. Zou
Physics Department, University of Alabama at Birmingham, Birmingham 35294, USA

coupling of the narrowband spectral response in the trapped resonances and the broadband spectral response in the stub resonators gives rise to the Fano resonance in the plasmonic structure. This phenomenon can be well explained by the analytic model and the relative phase analysis based on the scattering matrix theory. In sensing applications, calculations show that the sensitivity of the proposed structure is about $S=1.1\times10^3$ nm/RIU and its figure of merit is as high as 2×10^5 at $\lambda=980$ nm. This compact plasmonic structure with ultra-high figure of merits may find important applications in the on-chip nano-sensors.

Fano Resonances in the Simulation Model

The proposed plasmonic waveguide structure is schematically shown in Fig. 1, consisting of two identical stub resonators side-coupled with a MIM waveguide. This system is a two-dimensional model, and the gray and white parts in Fig. 1 denotes Ag and Air, respectively. The characteristics of the single stub resonator have been widely investigated before, and it typically exhibits broadband transmission spectra with nearly symmetric Lorentzian-like line-shapes [20–23, 26]. In the proposed structure, the two identical stub resonators would affect and couple with each other through the connection part of the MIM waveguide. This could greatly affect the line-shapes of the transmission spectra.

In order to investigate the influences, the transmission spectra of the proposed plasmonic structure are simulated with the finite element method (FEM) of COMSOL Multiphysics. In the simulations, the MIM dielectric gap, and the stub width and length are assumed to be $t=50$ nm, $w=50$ nm, and $d=500$ nm, respectively. For the MIM waveguide, the propagation length of the SPPs (e.g., ~40 μm at $\lambda=1{,}000$ nm) is much greater than the ultracompact device sizes (<1 μm), so the propagation loss will not cause large damping and has little influence on the device performance [21, 23, 26]. The transmittance of the SPPs in the MIM waveguide structure is defined as the quotient between the SPP power flows (obtained by integrating the Poynting vector over the cross section of the MIM waveguide) of the observing port with stubs and without stubs [23, 26]. The transmittance spectra of the proposed structure were obtained by changing the input wavelength of λ. The permittivity of Ag as a function of λ was taken from literature [30] and expanded by using the method of interpolation. This single stub resonator yields a broadband symmetric Lorentzian-like spectrum with a resonant wavelength of $\lambda_0=970$ nm and a bandwidth of $\Delta\lambda_{FWHM}\approx180$ nm, as shown by the black dashed lines in Fig. 2. It should be stressed that the choice of these structure parameters is arbitrary, and that the geometry of the stub resonator can always be tuned to match the desired wavelength. With regard to this Lorentzian-like response line-shapes, from the peak (corresponding to an "on" state) to the valley (corresponding to an "off" state), the wavelength separation or shift is about $\Delta\lambda=300$ nm. This indicates a low sensitivity of response spectra to the index variations of nearby or surrounding medium for the single stub resonator.

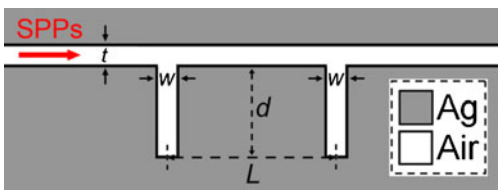

Fig. 1 Schematic and geometrical parameters of the MIM waveguide side-coupled with two identical stubs with exactly the same dimensions

For two coupling resonators with proper separations, the situation becomes considerably different because of the coupled-resonator effect. To display the difference, the transmission spectra of the plasmonic waveguide structure with two identical stubs are simulated for two typical separations (e.g., $L=300$ nm and $L=420$ nm), and the results are shown by the red solid lines in Fig. 2. Clearly, it is observed that the transmission spectra (red solid lines in Fig. 2) in the two coupling resonators become sharp and asymmetric, which is quite different from that in the single-resonator case. For the asymmetric spectra, the transmittance of the SPPs varies sharply from the valley to the peak with only a small wavelength shift of about $\Delta\lambda'=20$ nm (red lines in Fig. 2), which is considerably smaller than that ($\Delta\lambda=300$ nm) in the single-resonator case. This reveals that the wavelength shift required for a completely on/off variation is significantly reduced, implying a high sensitivity to the index variations of nearby or surrounding medium. The corresponding field distributions at the peak and valley positions for $L=420$ nm are displayed in Fig. 2c and d. At $\lambda=970$ nm, the SPPs are blocked by the stub resonators, and the output of the MIM waveguide is dark, as shown in Fig. 2c. At $\lambda=1001$ nm, strong field distributions are obviously observed in the FP resonator [Fig. 2d], which is attributed to the high reflectivity off the stub resonators. This serves as direct evidences that a strong trapped resonance occur in the FP resonator, resulting in a narrow transmission peak. Thus, the sharp and asymmetric spectra, usually termed as Fano resonances, result from the coupling of a narrow discrete resonance (strong trapped resonance in the FP resonator) and a broad spectrum (weak

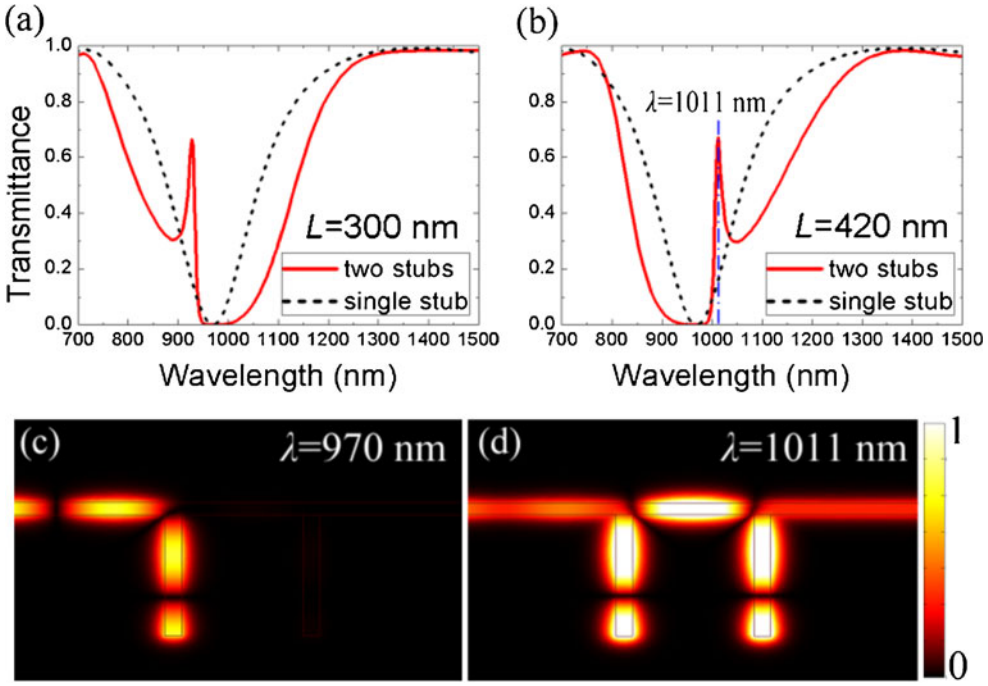

Fig. 2 Transmission spectra of two identical coupling stubs (*red solid lines*) and single resonator (*black dashed lines*) in the simulation models for **a** L=300 nm and **b** L=420 nm. Field distributions of the coupled-resonator structure with L=420 nm at **c** λ=970 nm and **d** λ=1,011 nm

resonance in the stub resonators) [1, 2]. The pronounced properties in the ultra-small structure, such as the high sensitivity to the index variations of nearby or surrounding medium as well as the strong field enhancements, can be exploitable in applications of nano-plasmonic sensing [1, 2, 12, 28, 29].

Sensing Applications Based on Fano Resonances

To verify the validity of exploitability in the applications, the sensing characteristics of the proposed structure are numerically calculated further, and the results are displayed in Fig. 3. It is observed that the Fano line-shapes has a red-shift of about 11 nm when the refractive index of the dielectric gap changes from n=1.00 to n=1.01, as displayed by the red dashed line in Fig. 3a. The sensitivity of a sensor (nm/RIU) is usually defined as the shift in the resonance wavelength per unit variations of the refractive index [28]. Thus, the sensitivity of the proposed structure is about S=1.1×10^3 nm/RIU. Considering that lasers are widely used in practice (one-wavelength output), a figure of merit (FOM) at a fixed wavelength can be defined as FOM* = $\Delta T/(T\Delta n)$ [31, 32], where T denotes the transmittance in the proposed structure. From this equation, we can get that an ultra-low transmittance (T) and a sharp change ($\Delta T/\Delta n$) of the transmittance induced by index variations can result in a large value of FOM*. The calculated FOM* is shown in Fig. 3b. It is observed that the FOM* is as high as 2×10^5 at λ=980 nm, which is due to the sharp asymmetric Fano line-shape with ultra-low transmittance at this wavelength, as shown in Fig. 3a. Moreover, it is noted that the FOM* is greater than 1,000 in the wavelength range of 975 to 1,005 nm, as shown by the inset in Fig. 3b. These FOM* values are significantly greater than that in the previous reports (24 in [32] and 500 in [29]).

Fano Resonances in the Analytic Model

To test the simulation results above, an analytic model based on the scattering matrix theory [33] is used to explain the transmission spectra in the proposed system. Quantitatively, the scattering property of the single stub resonator for the incident SPPs at a frequency of $\omega = c/\lambda$ can be given by a transfer matrix of T_S [23, 26, 33],

$$\begin{bmatrix} A_{Ob} \\ A_{Ib} \end{bmatrix} = T_S \begin{bmatrix} A_{Ia} \\ A_{Oa} \end{bmatrix} = \begin{bmatrix} 1-\frac{i\delta}{\omega-\omega_0} & \frac{-i\delta}{\omega-\omega_0} \\ \frac{i\delta}{\omega-\omega_0} & 1+\frac{i\delta}{\omega-\omega_0} \end{bmatrix} \begin{bmatrix} A_{Ia} \\ A_{Oa} \end{bmatrix}, \quad (1)$$

where, c is the velocity of light in vacuum; $\omega_0 = c/\lambda_0$ and $2\delta = c\Delta\lambda_{FWHM}/\lambda_0^2$ are the resonant frequency and bandwidth of the stub resonator (coupled with the MIM waveguide), respectively; A_{Ij} and A_{Oj} (j = a, b) are the incoming and outgoing SPP amplitudes on one side of the stub resonator.

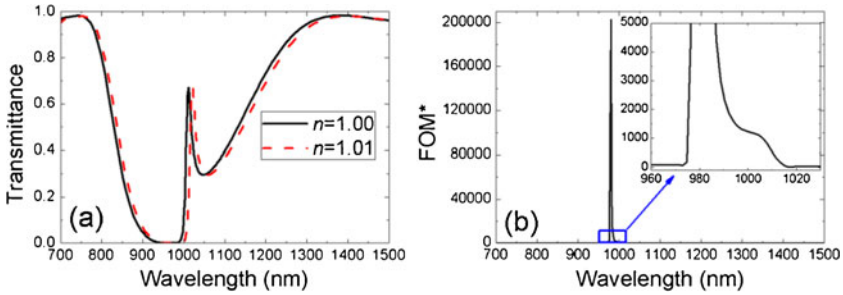

Fig. 3 **a** Transmission spectra of two identical coupling stubs with L=420 nm for dielectric gap of different refractive index in sensing applications. **b** Calculated FOM* at different wavelengths. *Inset* shows the detailed FOM*

For the phase shift coming from the SPPs propagating from the one stub to the other stub along the MIM waveguide, the transfer matrix T_P has the form of [23, 26, 33]

$$T_P = \begin{bmatrix} \exp(i\varphi) & 0 \\ 0 & \exp(-i\varphi) \end{bmatrix}, \quad (2)$$

where, $\varphi = 2\pi n_{eff} L/\lambda$ is the accumulated phase shift for the SPPs propagating from one stub to the other stub; L is the separation between the two stubs; and n_{eff} is the effective refractive index of SPPs in the MIM waveguide. Therefore, the transfer matrix of T_{all} for the coupled-resonator system can be expressed as

$$T_{all} = T_S \times T_P \times T_S. \quad (3)$$

As a consequence, the transmittance in the system is determined by $|1/T_{all,22}|^2$. The calculated transmission spectra of the coupled-resonator systems using the analytic model are displayed in Fig. 4. It is observed that these results agree well with the FEM simulation results. In the calculations, $n_{eff} \approx 1.38+0.002i$ was obtained from the FEM simulations at λ=1,000 nm; and the resonant wavelength and bandwidth of the stub resonator are 970 nm and $\Delta\lambda_{FWHM}$ = 180 nm, respectively. The slight deviation is due to the dispersion [34] as well as the propagation loss and coupling loss varying with wavelengths [35] in the MIM waveguide, which are not included in the analytic model.

Moreover, from Eq. (1), we can get that the stub resonator can reflect SPPs with a amplitude reflectivity of $r_s = |T_{S,21}/T_{S,22}|$ and a phase shift of θ = arctan [Im($T_{S,21}/T_{S,22}$)/Re($T_{S,21}/T_{S,22}$)]. Thus, the SPPs can be reflected back and forth off the two stubs, constructing an FP resonator [18]. The accumulated phase delay per round trip in the FP resonator is

$$\varphi(\lambda, L) = 4\pi n_{eff} L \Big/ \lambda + 2\theta. \quad (4)$$

According to Eq. (4), constructive interferences should occur when $\varphi(\lambda,L)$ is equal to $2m\pi$ (m being integer). It is easily obtained that $\varphi(\lambda$=937 nm, L=300 nm) = $\varphi(\lambda$=1,001 nm, L=400 nm) = 2π. This reveals a constructive interference in the FP resonator, exciting strong trapped resonances and giving rise to the transmission peaks at these wavelengths, as shown in Fig. 4. It should be pointed out that the relative phase analysis agrees well with both of the simulation model and analytical model.

Conclusion

In summary, Fano resonances in an MIM waveguide coupled with two identical stub resonators were numerically predicted. Near the resonant wavelength of the stub resonator, the surface plasmon polaritons guided by the MIM waveguide are highly reflected back and forth by the stub resonators, exciting strong trapped resonances with narrow bandwidths. The coupling of the narrowband spectral response in the trapped resonances and the broadband spectral response in the stub resonators gives rise to the Fano resonance. An analytic model and the relative phase analysis based on the scattering matrix theory were used to explain this phenomenon, which matched well with the FEM simulation results. Therefore, the analytical model and the relative phase analysis can facilitate designing compact and complex functional plasmonic devices. In sensing applications, the sensitivity of the proposed structure with footprints of only

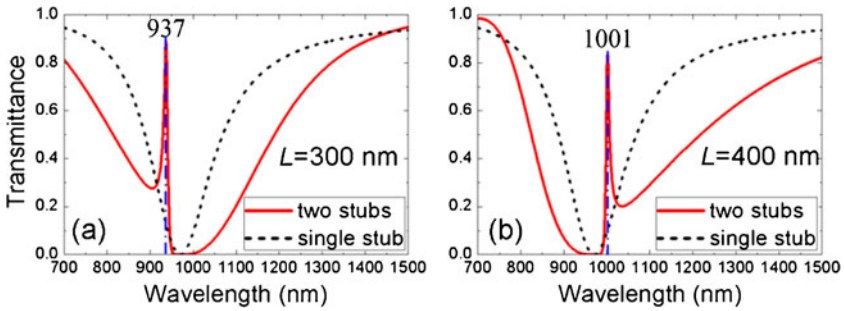

Fig. 4 Transmission spectra of two identical coupling stubs (*red solid lines*) and single resonator (*black dashed lines*) in the analytic model for **a** L= 300 nm and **b** L=400 nm

about 0.2 μm^2 is about $S=1.1\times10^3$ nm/RIU and its figure of merit is as high as 2×10^5 at $\lambda=980$ nm. This is of importance in on-chip nano-plasmonic sensors.

Acknowledgments This work was supported by the National Natural Science Foundation of China (Grant nos. 11204018, 61177085, and 51172030) and the National Basic Research Program of China (Grants 2010CB923200, 2009CB930504, and 2013CB328704).

References

1. Miroshnichenko E, Flach S, Kivshar YS (2010) Fano resonances in nanoscale structures. Rev Mod Phys 82(3):2257–2298
2. Luk'yanchuk B, Zheludev NI, Maier SA, Halas NJ, Nordlander P, Giessen H, Chong CT (2010) The Fano resonance in plasmonic nanostructures and metamaterials. Nat Mater 9(9):707–715
3. Verellen N, Sonnefraud Y, Sobhani H, Hao F, Moshchalkov VV, Van Dorpe P, Nordlander P, Maier SA (2009) Fano resonances in individual coherent plasmonic nanocavities. Nano Lett 9:1663–1667
4. Chen JJ, Li Z, Zhang X, Xiao JH, Gong QH (2013) Submicron bidirectional all-optical plasmonic switches. Sci Rep 3:1451. doi:10.1038/srep01451, Published online 2013 March 14
5. Fedotov VA, Rose M, Prosvirnin SL, Papasimakis N, Zheludev NI (2007) Sharp trapped-mode resonances in planar metamaterials with a broken structural symmetry. Phys Rev Lett 99:147401
6. Christ A, Martin OJF, Ekinei Y, Gippius NA, Tikhodeev SG (2008) Symmetry breaking in a plasmonic metamaterial at optical wavelength. Nano Lett 8:2171–2175
7. Christ A, Ekinei Y, Solak HH, Gippius NA, Tikhodeev SG, Martin OFJ (2007) Controlling the Fano interference in a plasmonic lattice. Phys Rev B 76:201405
8. Liu N, Kaiser S, Giessen H (2008) Magnetoinductive and electroinductive coupling in plasmonic metamaterial molecules. Adv Mater 20:4521–4525
9. Liu N, Langguth L, Weiss T, Kastel J, Fleischhauer M, Pfau T, Giessen H (2009) Plasmonic analogue of electromagnetically induced transparency at the Drude damping limit. Nat Mater 8:758–762
10. Zhang S, Genov DA, Wang Y, Liu M, Zhang X (2008) Plasmon-induced transparency in metamaterials. Phys Rev Lett 101:047401
11. Hentschel M, Saliba M, Vogelgesang R, Giessen H, Alivisatos AP, Liu N (2010) Transition from isolated to collective modes in plasmonic oligomers. Nano Lett 10:2721–2726
12. Liu N, Weiss T, Mesch M, Langguth L, Eigenthaler U, Hirscher M, Sönnichsen C, Giessen H (2010) Planar metamaterial analogue of electromagnetically induced transparency for plasmonic sensing. Nano Lett 10:1103–1107
13. Aydin K, Pryce IM, Atwater HA (2010) Symmetry breaking and strong coupling in planar optical metamaterials. Opt Express 18:13407–13417
14. Artar A, Yanik AA, Altug H (2011) Multispectral plasmon-induced transparency in coupled meta-atoms. Nano Lett 11:1685–1689
15. Hentschel M, Dregely D, Vogelgesang R, Giessen H, Liu N (2011) Plasmonic oligomers: the role of individual particles in collective behavior. Acs Nano 5:2042–2050
16. Rahmani M, Lukiyanchuk B, Ng B, Tavakkoli KGA, Liew YF, Hong MH (2011) Generation of pronounced Fano resonances and tuning of subwavelength spatial light distribution in plasmonic pentamers. Opt Express 19:4949–4956
17. Zhang J, Bai WL, Cai LK, Xu Y, Song GF, Gan QQ (2011) Observation of ultra-narrow band plasmon induced transparency based on large-area hybrid plasmon-waveguide systems. Appl Phys Lett 99:181120
18. Kekatpure RD, Barnard ES, Cai W, Brongersma M (2010) Phase-coupled plasmon-induced transparency. Phys Rev Lett 104:243902
19. He YR, Zhou H, Jin Y, He SL (2011) Plasmon induced transparency in a dielectric waveguide, Appl Phys Lett 99:043113
20. Zhang Y, Darmawan S, Tobing LYM, Mei T, Zhang DH (2011) Coupled resonator-induced transparency in ring-bus-ring Mach–Zehnder interferometer. J Opt Soc Am B 28(1):28–36
21. Chen JJ, Li Z, Yue S, Gong QH (2011) Compact and high–resolution plasmonic wavelength demultiplexers based on Fano interference. Opt Express 19:9976–9985
22. Han Z, Bozhevolnyi SI (2011) Plasmon-induced transparency with detuned ultracompact Fabry–Perot resonators in integrated plasmonic devices. Opt Express 19:3251–3257
23. Chen JJ, Li Z, Lei M, Fu XL, Xiao JH, Gong QH (2012) Plasmonic y-splitters of high wavelength resolution based on strongly-coupled-resonator effects. Plasmonics 7:441–445
24. Piao X, Yu S, Park N (2012) Control of Fano asymmetry in plasmon induced transparency and its application to plasmonic waveguide modulator. Opt Express 20(17):18994–18999
25. Lu H, Liu XM, Mao D, Gong YK, Wang GX (2011) Induced transparency in nanoscale plasmonic resonator systems. Opt Lett 36:3233–3235
26. Chen JJ, Wang C, Zhang R, Xiao JH (2012) Multiple plasmon-induced transparencies in coupled-resonator systems. Opt Lett 37:5133–5135
27. Wang G, Lu H, Liu X (2012) Dispersionless slow light in MIM waveguide based on a plasmonic analogue of electromagnetically induced transparency. Opt Express 20:20902–20907
28. Chen JJ, Li Z, Yue S, Xiao JH, Gong QH (2012) Plasmon-induced transparency in asymmetric T-shape single slit. Nano Lett 12:2494–2498
29. Lu H, Liu X, Mao D, Wang G (2012) Plasmonic nanosensor based on Fano resonance in waveguide-coupled resonators. Opt Lett 37:3780–3782
30. Johnson PB, Christy RW (1972) Optical constants of the noble metals. Phys Rev B 6:4370–4379
31. Ameling R, Langguth L, Hentschel M, Mesch M, Braun PV, Giessen H (2010) Cavity-enhanced localized plasmon resonance sensing. Appl Phys Lett 97:253116
32. Becker J, Truegler A, Jakab A, Hohenester U, Soennichsen C (2010) The optimal aspect ratio of gold nanorods for plasmonic bio-sensing. Plasmonics 5:161
33. Haus HA (1984) Waves and fields in optoelectronics. Prentice Hall, New York
34. Economou EN (1969) Surface plasmons in thin films. Phys Rev 182(2):539–554
35. Veronis G, Fan S (2005) Bends and splitters in metal–dielectric–metal subwavelength plasmonic waveguides. Appl Phys Lett 87:131102